Uludağ University Journal of The Faculty of Engineering, Vol. 24, No. 2, 2019 RESEARCH

DOI: 10.17482/uumfd.548410

DESIGN and ANALYSIS of 28 GHz MICROSTRIP PATCH ANTENNA for DIFFERENT TYPE FR4 CLADDINGS

Bahadır HİÇDURMAZ [*]
Ömer Faruk GÜMÜŞ [*]

Received: 02.04.2019; revised: 20.05.2019; accepted: 23.05.2019

Abstract: In this study, rectangular patch microstrip antennas operating at 28 GHz frequency compatible with 5G mobile technology are designed with Computer Simulation Technology (CST) program for different patch materials and the performances of the designed antennas are compared. For each of the same sized antennas designed with the selected patch materials, it is found that they are suitable for the 28 GHz band and the best return loss performance is obtained by using the tantalum conductor while the silver conductor has the best antenna efficiency.

Keywords: 5G, rectangular patch microstrip antenna, different patch materials, CST design.

Farklı Tipte FR4 Kaplamaları için 28 GHz Mikroşerit Yama Anteni Tasarımı ve Analizi

Öz: Bu çalışmada, 5G mobil teknolojisine uygun olarak 28 GHz frekansında çalışan dikdörtgen yama mikroşerit antenler, farklı yama malzemeleri için Computer Simulation Technology (CST) programı ile tasarlanmış ve tasarlanan antenlerin performansları karşılaştırılmıştır. Seçilen yama malzemeleri ile tasarlanan aynı boyuttaki antenlerin her biri için 28 GHz bandında çalışmalarının uygun oldukları ve en iyi geri dönüş performansının tantal iletkeninin kullanılması ile elde edilirken gümüş iletkenin en iyi anten verimine sahip olduğu görülmüştür.

Anahtar Kelimeler: 5G, dikdörtgen yama mikroşerit anten, farklı yama malzemeleri, CST tasarım.

1. INTRODUCTION

5th generation (5G) mobile technology (Rodriguez, 2015) greatly increases the communication capacity. This innovation brings the need for advanced antenna design. Performing an antenna with high gain, low loss, low cost, high bandwidth, and high radiation efficiency leads to various design considerations (Balanis, 2016).

Modern wireless communication systems require low-profile, lightweight, high-gain and simple-built antennas to ensure reliability, mobility and high efficiency. Therefore, microstrip antennas are highly preferred due to their low profile, simple to manufacture, and ease of feeding. In recent years, there are quite a few microstrip antenna designs in different structures in the literature. Islam et. al. (2016) designed a microstrip patch antenna for the WiMAX communication system operating in the 5.8 GHz frequency band and they evaluated the performance for different dielectric material. The best performance was observed for FR4 and

[*] Dumlupınar Üniversitesi, Mühendislik Fakültesi, Elektrik-Elektronik Mühendisliği Bölümü, 43100 Evliya Çelebi Yerleşkesi, Kütahya
İletişim Yazarı: Bahadır Hiçdurmaz (bahadir.hicdurmaz@dpu.edu.tr)

dupont-951 dielectric materials. Yoon and Seo, 2017 proposed a 2x2 U-slotted array antenna operating at 28 GHz for the broadband communication system. In their studies, they achieved about 3.35 GHz bandwidth and about 13 dBi gain in this operating frequency. A small microstrip patch antenna was implemented for the 5G wireless standard using High-Frequency Structure Simulator (HFSS) in Verma et. al. (2016). From the measured results, it was observed that the designed antenna resonates at 10.11 GHz with a bandwidth of 380 MHz. In Khalily et. al. (2016), the modified serial-feed patch antenna array is designed and implemented for 28 GHz millimeter wave applications. The proposed designs are predicted to be applicable for future 5G. Kiran et. al. (2018) investigated a compact elliptical microstrip patch antenna operating at 28 GHz by using a simulation program and obtained good results. Ahmed et. al. (2017) performed on the sloped substrate of the mm-wave microstrip patch array. The convex slope of the substrate was observed to be highly effective on performance, while the concave slope was observed to have a minimal effect. Sethi et. al. (2018) achieved an average gain of approximately 23 dBi in the broadband range (25-40 GHz) operating at 28 GHz and 38 GHz, by designing a 4 x 4 slot-coupled Vivaldi antenna (SCVA) array unit cell. Parchin et. al. (2016) simulated an end-fire-phase array 5G antenna design with the Arlon AR 350 substrate and obtained good performances in the 28 GHz and 38 GHz bands. In the research of Mahabub et. al. (2018) related to the subject, a multi-band patch antenna was designed using the CST Microwave Studio software for 2.4 GHz Wi-Fi, 7.8 GHz WiMAX and 33.5 GHz 5G communications applications. The designed antenna exhibited low Voltage Standing Wave Ratio (VSWR) and high directivity at operating frequencies. Aguni et.al. (2019) designed a microstrip patch antenna for 2.45 GHz Industrial, Scientific and Medical (ISM) band applications using artificial neural network and obtained a good reflection coefficient value at desired frequency band. Bhanumathi and Swathi (2019) realized a compact inverted L-shaped patch antenna with a U-slot. The antenna operated from 4.8 to 7.8 GHz frequency band for UWB applications. Mondal and Sarkar (2019) recommended a high-gain wide-band microstrip patch antenna applicable for various applications such as satellite communication, WiMAX, scientific and medical band, etc. In their studies, it was achieved a peak gain of 9 dBi at 5.5-7.5 GHz frequency range through recommended antenna.

In the light of relevant literature it is our believe that the performance of a microstrip patch antenna for different patch and ground layer materials has not been studied yet. Therefore, in this study, the performance analysis of a microstrip patch antenna with FR-4 dielectric material operating in 28 GHz band for different patch and ground materials was performed by Computer Simulation Technology (CST)-program.

2. CONVENTIONAL MICROSTRIP PATCH ANTENNA (MPA) DESIGN

A microstrip antenna in its simplest form is a type of antenna with a radiating patch on one side of a dielectric substrate and a ground plane on the other side, as illustrated in Figure 1. Normally, copper and gold-made patch conductors can actually be in any form. For ease of analysis, the patch can practically be in familiar shapes like square, rectangular, circular, triangular, and the like. Furthermore, a variety of substrate types have been developed with various dielectric constant and loss tangent values (Garg et. al. 2001).

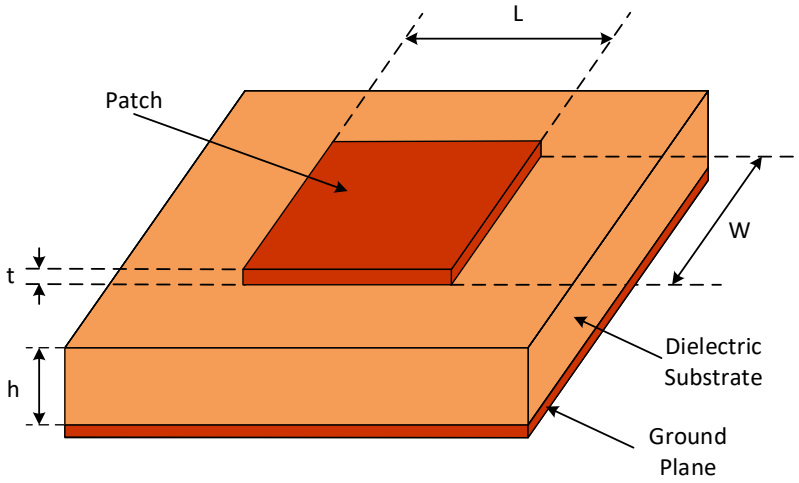

Figure 1:
The structure of a microstrip rectangular patch antenna

For a rectangular patch, the patch length L is generally between $\lambda_0/3$ and $\lambda_0/2$ where λ_0 is the wavelength of free space. The patch thickness t is chosen to be very thin such that $t << \lambda_0$. In general, the substrate height h is $0.003\lambda_0 \leq h \leq 0.05\lambda_0$. The dielectric constant of the substrate ε_r is ordinarily in the range of 2.2 to 12 (Balanis, 2016).

In order to get efficient radiation, a practical rectangular patch width W can be given as

$$W = \frac{c}{2 f_r} \sqrt{\frac{2}{\varepsilon_r + 1}} \tag{1}$$

where f_r is the resonant frequency of the antenna and c is the speed of light in vacuum. The effective dielectric constant of rectangular patch antenna ε_{reff} is expressed as

$$\varepsilon_{reff} = \frac{\varepsilon_r + 1}{2} + \frac{\varepsilon_r - 1}{2} \left(\frac{1}{\sqrt{1 + \frac{12h}{W}}} \right) \qquad \text{for} \quad \frac{W}{h} > 1. \tag{2}$$

Due to the fringing effects, the effective length L_{eff} is obtained as

$$L_{eff} = \frac{c}{2 f_r \sqrt{\varepsilon_{reff}}}. \tag{3}$$

The actual length of the patch is determined by

$$L = L_{eff} - 2\Delta L \tag{4}$$

where ΔL is extension length and given by

$$\Delta L = 0.412h \frac{\left(\varepsilon_{reff} + 0.3\right)\left(\frac{W}{h} + 0.264\right)}{\left(\varepsilon_{reff} - 0.258\right)\left(\frac{W}{h} + 0.8\right)}. \quad (5)$$

In order to operate a microstrip antenna, there are number of feeding techniques such as microstrip feed, inset feed, coaxial feed, proximity-coupled microstrip feed, aperture-coupled microstrip feed and coplanar waveguide feed. The choice of feeding technique depends on various factors. The most important one is the efficient transfer of power between the radiating structure and feeding structure. The structure of the inset feed microstrip patch is shown in Figure 2.

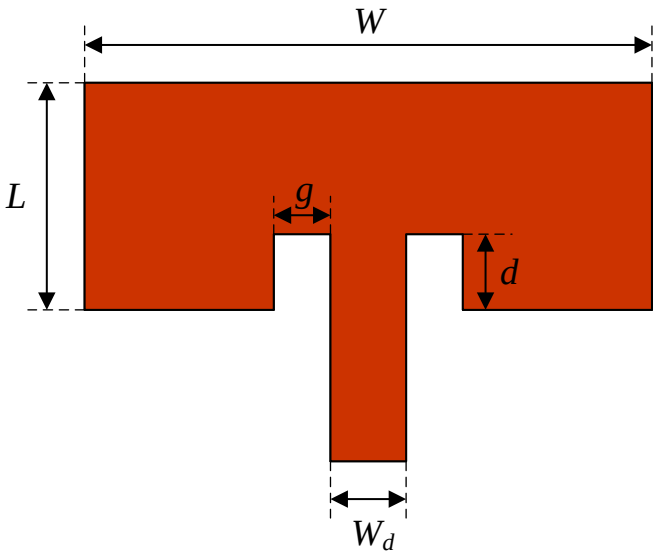

Figure 2:
The structure of the inset feed microstrip patch

Here, the characteristic impedance of the microstrip feeding line is given as follows:

$$Z_0 = \begin{cases} \dfrac{60}{\sqrt{\varepsilon_{reff}}} ln\left(\dfrac{8h}{W_d} + \dfrac{W_d}{4h}\right) & for \ \dfrac{W_d}{h} \le 1 \\ \dfrac{120\pi}{\sqrt{\varepsilon_{reff}}\left[\dfrac{W_d}{h} + 1.393 + 0.667 ln\left(\dfrac{W_d}{h} + 1.444\right)\right]} & for \ \dfrac{W_d}{h} \ge 1 \end{cases} \quad (6)$$

Then, the following statement can be obtained (Pozar, 2012).

$$\frac{W_d}{h}=\begin{cases}\dfrac{8e^{A}}{8e^{2A}-2} & for\ \dfrac{W_d}{h}<2\\[2ex] \dfrac{2}{\pi}\left[B-1-ln\left(2B-1\right)+\dfrac{\varepsilon_r-1}{2\varepsilon_r}\left\{ln\left(B-1\right)+0.39-\dfrac{0.61}{\varepsilon_r}\right\}\right] & for\ \dfrac{W_d}{h}>2\end{cases} \quad (7)$$

where $A=\dfrac{Z_0}{60}\sqrt{\dfrac{\varepsilon_r+1}{2}}+\dfrac{\varepsilon_r-1}{\varepsilon_r+1}\left(0.23+\dfrac{0.11}{\varepsilon_r}\right)$ and $B=\dfrac{377\pi}{2Z_0\sqrt{\varepsilon_r}}$

The input resistance for most typical inset-feed microstrips is given as (Balanis, 2016)

$$R_{in}=\frac{1}{2(G_1\pm G_{12})}\cos^2(\frac{\pi}{L}d)\,. \quad (8)$$

Here, G_1 is the conductance of the patch in its transmission line model while G_{12} is the mutual conductance due to mutual effects between the slots. These quantities are given below.

$$G_1=\frac{I_1}{120\pi^2} \quad (9)$$

$$G_{12}=\frac{1}{120\pi^2}\int_0^{\pi}\left[\frac{\sin\left(\frac{k_0W}{2}\cos\theta\right)}{\cos\theta}\right]^2 J_0(k_0L\sin\theta)\sin^3\theta\,d\theta \quad (10)$$

In here, k_0 is phase constant for free space and

$$I_1=\int_0^{\pi}\left[\frac{\sin\left(\frac{k_0W}{2}\cos\theta\right)}{\cos\theta}\right]^2\sin^3\theta\,d\theta \quad (11)$$

$$= -2+\cos(k_0W)+(k_0W)\,S_i(k_0W)+\frac{\sin(k_0W)}{(k_0W)}$$

where $S_i(x)$ is the sine integral function defined as $S_i(x) = \int_0^x \frac{\sin(t)}{t}\, dt$.

For inset-feed microstrip patch, notch width g can be formulated as (Matin, 2010)

$$g = \frac{4.65 \times 10^{-9} c}{f_r \sqrt{2\varepsilon_{reff}}} \tag{12}$$

Lastly, the minimum dimensions of the ground plane, L_{g_min} and W_{g_min} can be given as (Nakar, 2004)

$$L_{g\_min} = 6h + L \tag{13}$$

$$W_{g\_min} = 6h + W \tag{14}$$

3. SIMULATION RESULTS OF DESIGNED ANTENNAS

In this study, FR-4 with a dielectric constant of 4.3 was selected as a dielectric substrate and its height was 0.1 mm. According to these values and the resonant frequency of 28 GHz, W and L dimensions of the patch obtained from theoretical formulas were approximately 3.29 mm and 2.44 mm, respectively. In each designed antennas, inset microstrip feeding was used. The structure of antennas designed by using the CST is shown in Figure 3. From the formulas through 1-14, it was obtained as the inset feeding length, d = 0.95 mm, the width of feed length, W_d = 0.194 mm, notch width, g = 0.0174 mm, the minimum dimensions of the ground plane, L_{g_min} = 6 mm and W_{g_min} = 6 mm.

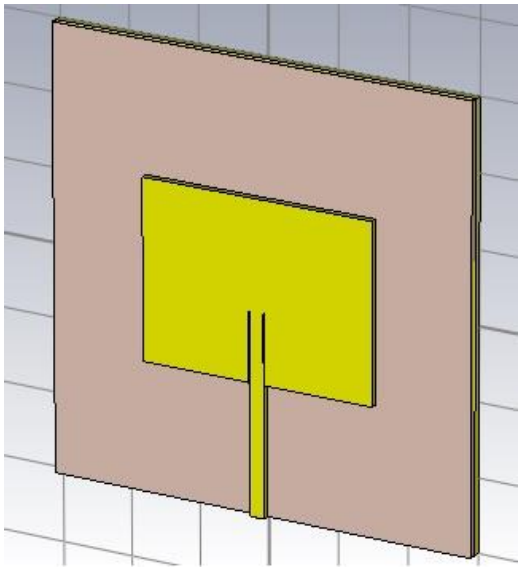

Figure 3:
The structure of the designed antennas

The designs were realized for copper, aluminum, gold, silver, iron, platinum, tantalum and molybdenum conductors, respectively. The return loss graphs obtained for these designs are shown in Figures 4-11, respectively. Then, the results are listed in Table 1 for evaluation.

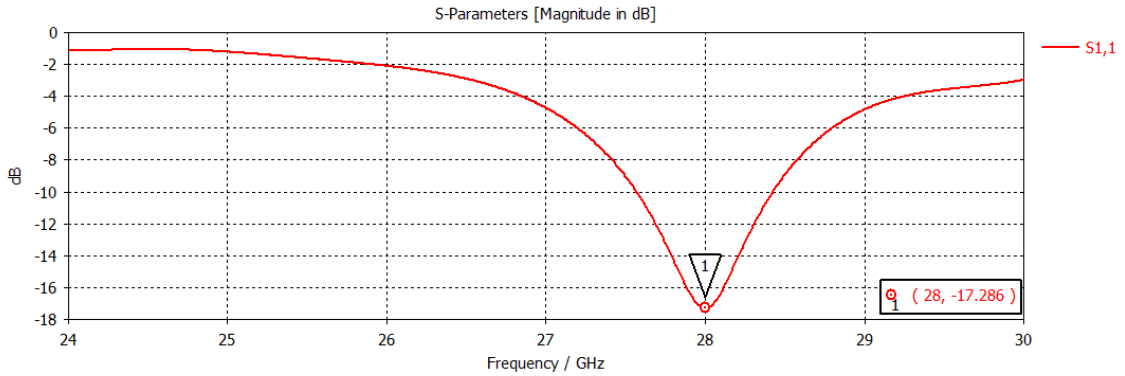

Figure 4:
The return loss graph for copper conductor

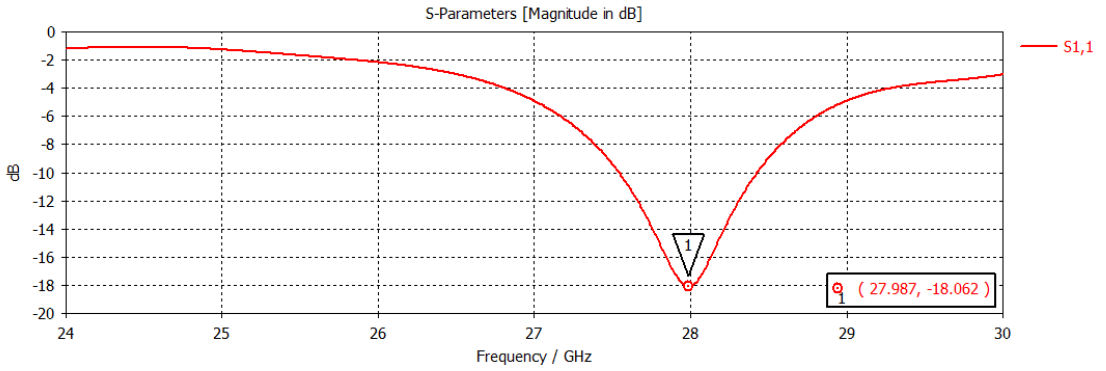

Figure 5:
The return loss graph for aluminum conductor

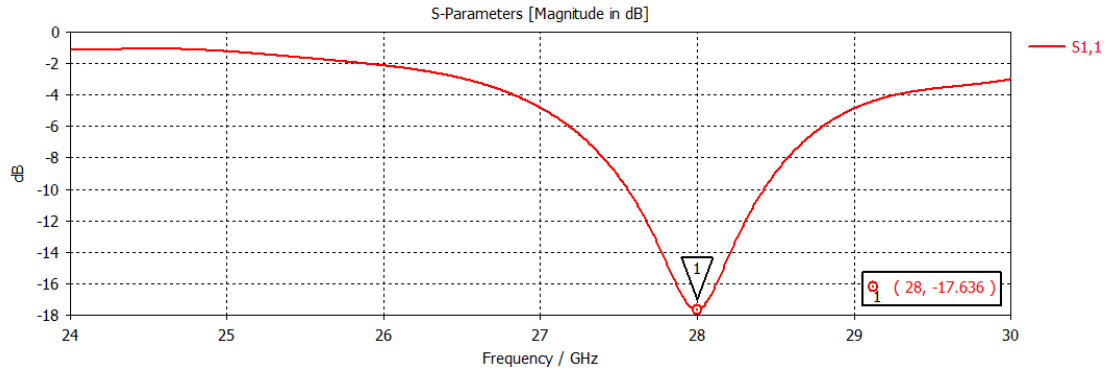

Figure 6:
The return loss graph for gold conductor

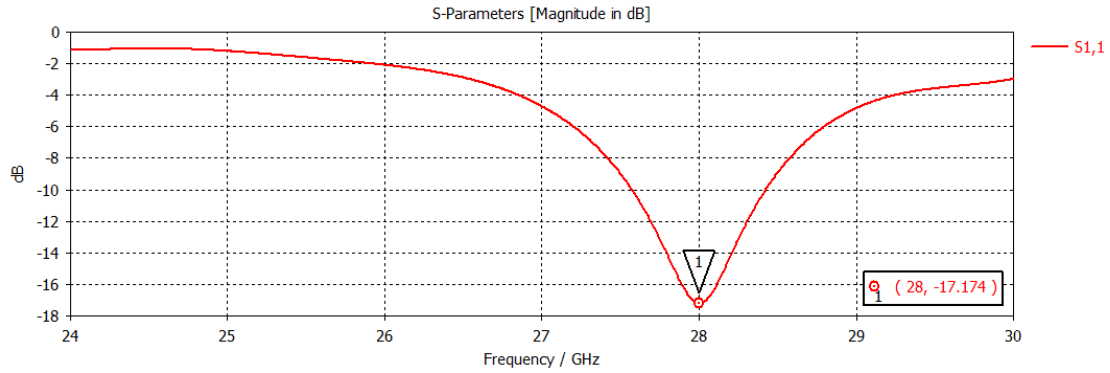

Figure 7:
The return loss graph for silver conductor

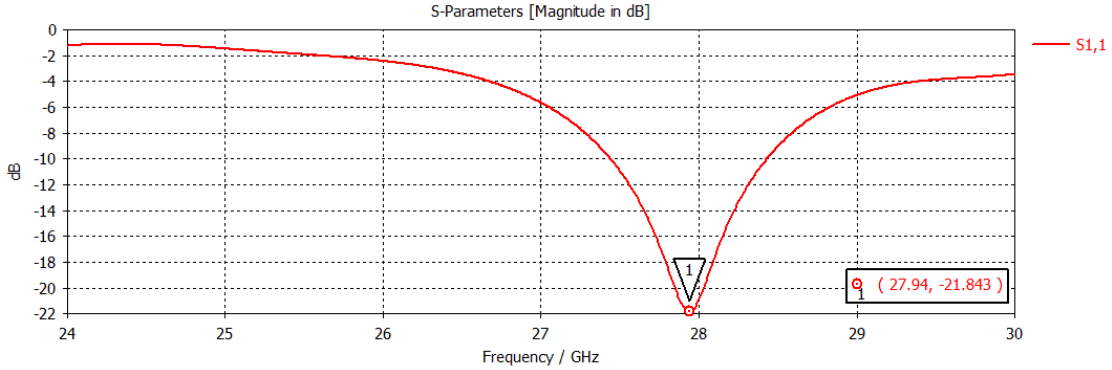

Figure 8:
The return loss graph for iron conductor

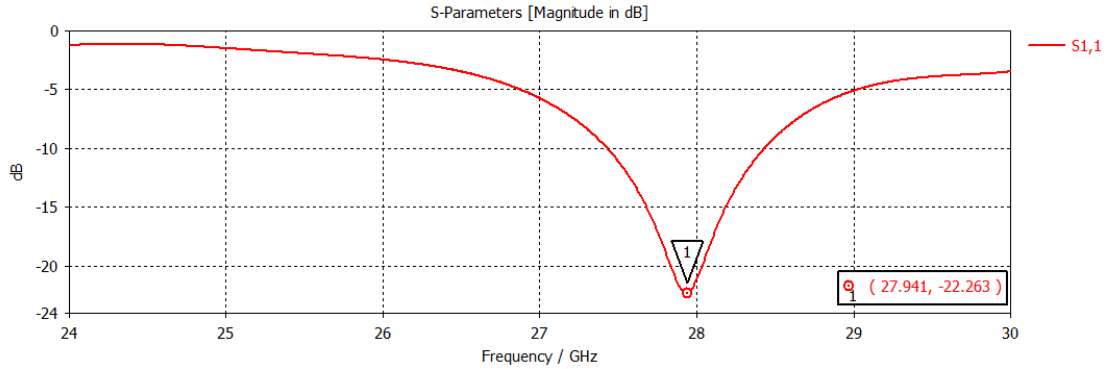

Figure 9:
The return loss graph for platinum conductor

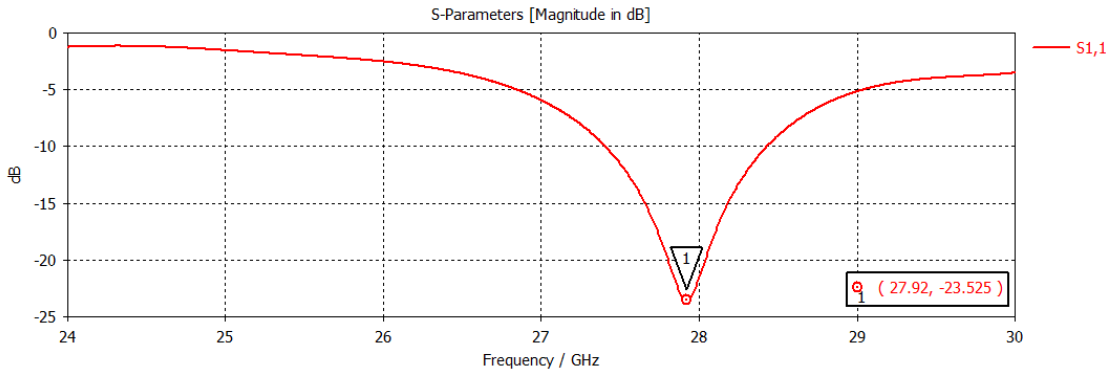

Figure 10:

The return loss graph for tantalum conductor

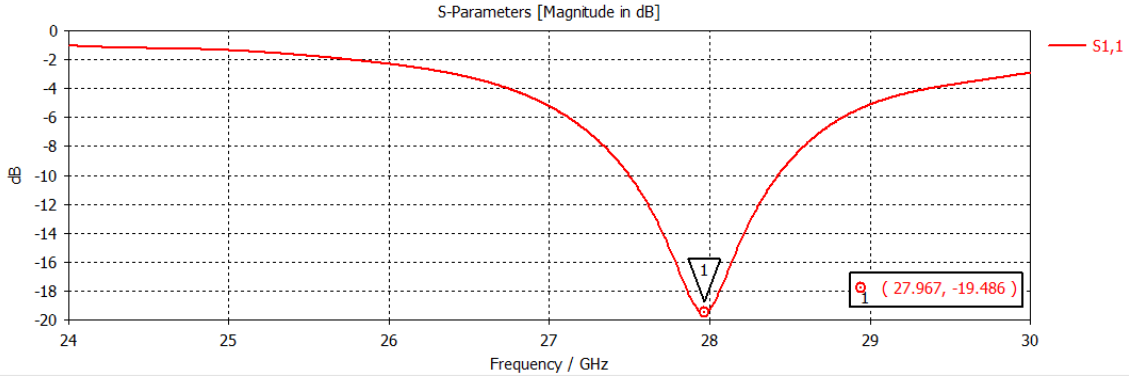

Figure 11:

The return loss graph for molybdenum conductor

Table 1. Comparison of antennas with different patch and ground conductors for resonant frequency and S_{11} values.

	Copper	Aluminum	Gold	Silver	Iron	Platinum	Tantalum	Molybdenum
Resonant Frequency (GHz)	28	27.987	28	28	27.94	27.941	***27.92***	27.967
S_{11}(dB)	-17.28	-18.062	-17.63	-17.17	-21.84	-22.263	***-23.525***	-19.486

According to these results, the tantalum conductor provided the best return loss value at a resonance frequency around 28 GHz. The far-field patterns in 3 dimensional and 2 dimensional (phi=90° and theta=90°) of the antennas designed for different patch conductors are presented in Figures 12-19, respectively.

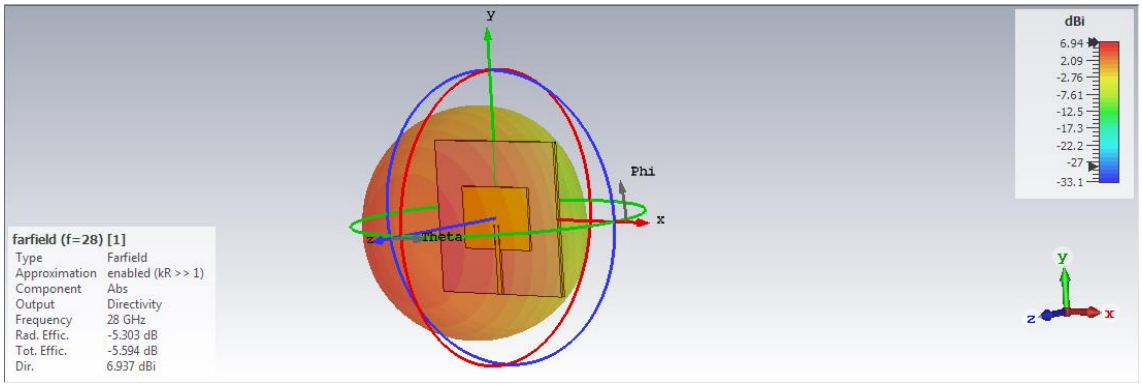

Figure 12-a

The far-field pattern in 3 dimensional of the antenna with copper cladding

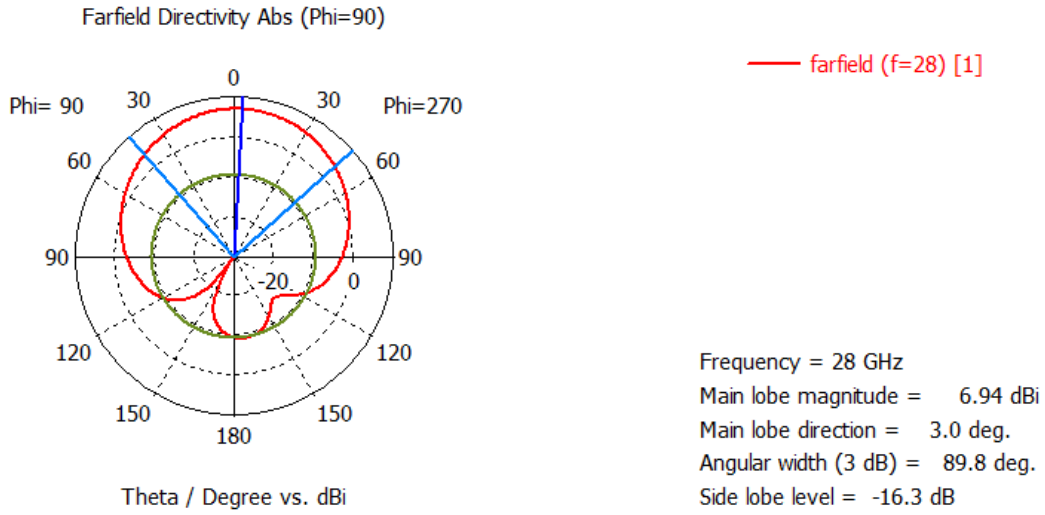

Figure 12-b

The far-field pattern in 2 dimensional (phi=90°) of the antenna with copper cladding

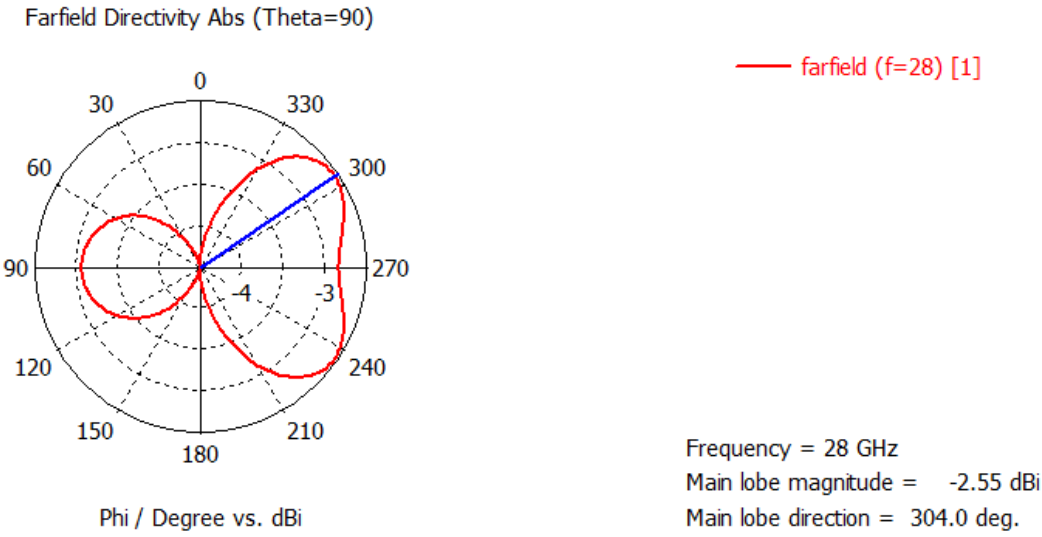

Figure 12-c

The far-field pattern in 2 dimensional (theta=90°) of the antenna with copper cladding

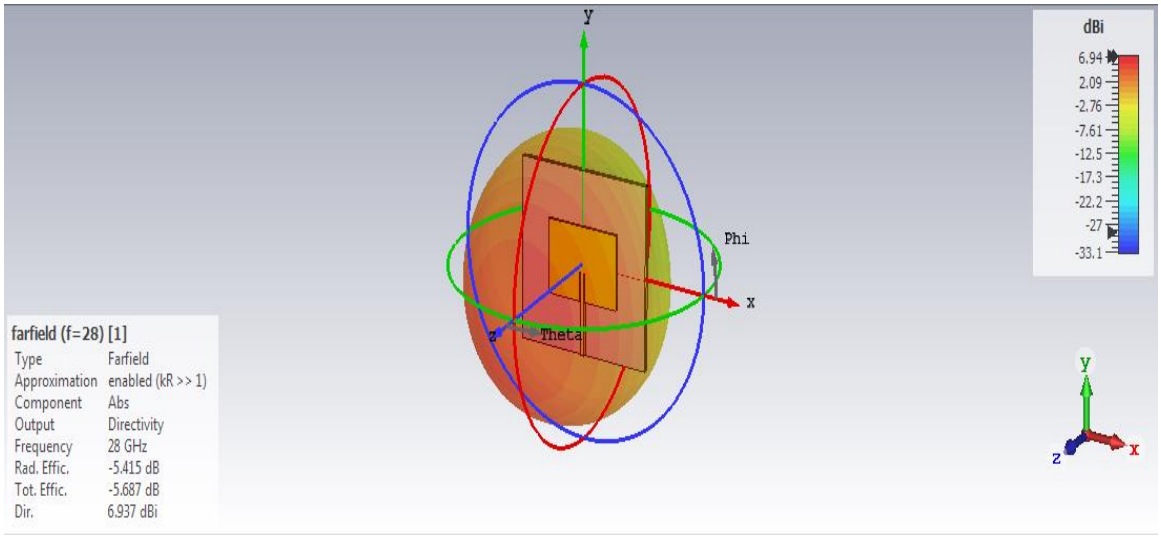

Figure 13-a

The far-field pattern in 3 dimensional of the antenna with aluminum cladding

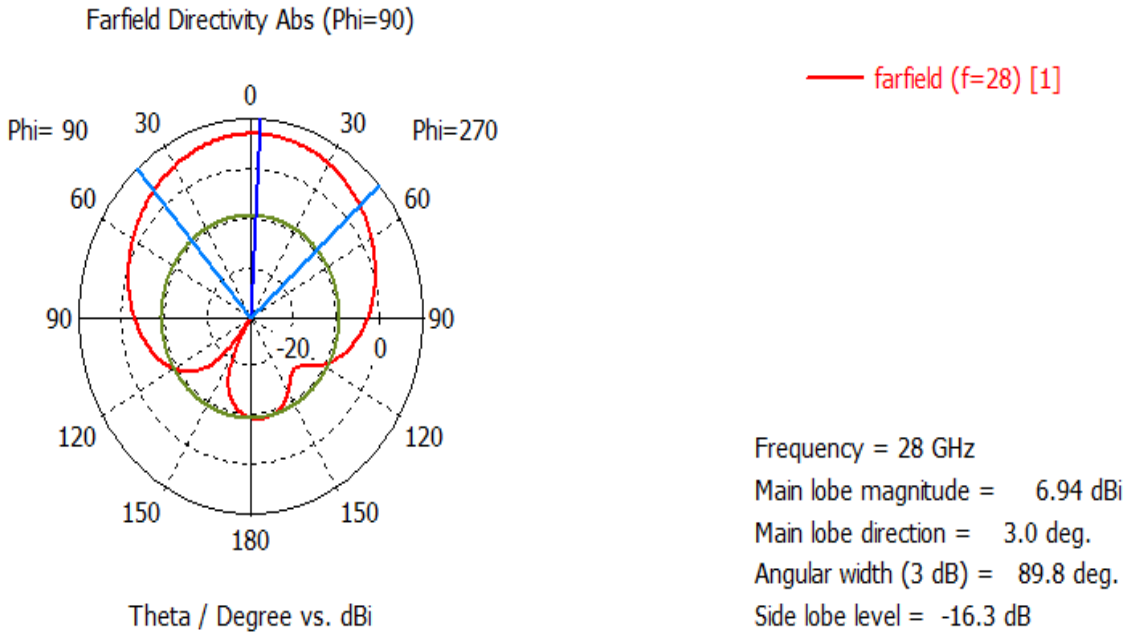

Figure 13-b

The far-field pattern in 2 dimensional (phi=90°) of the antenna with aluminum cladding

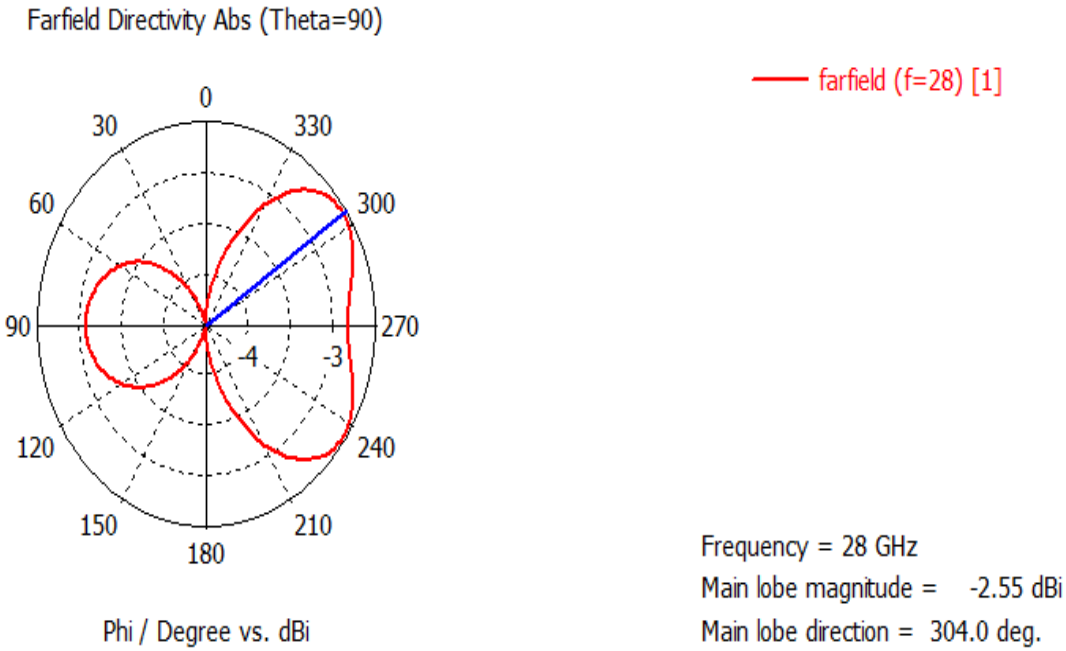

Figure 13-c

The far-field pattern in 2 dimensional (theta=90°) of the antenna with aluminum cladding

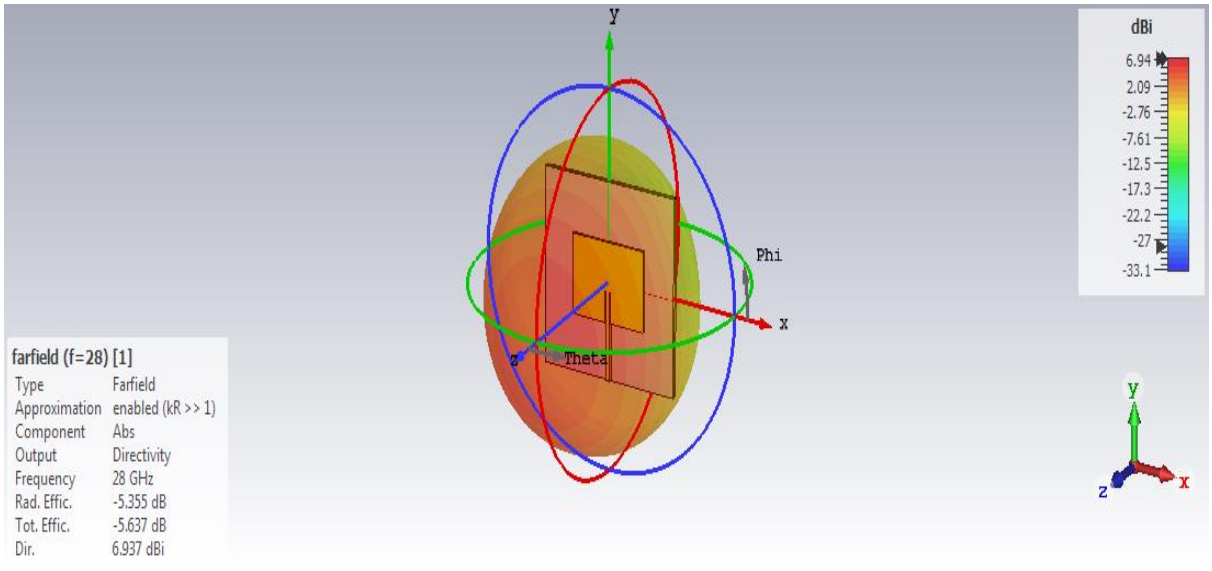

Figure 14-a

The far-field pattern in 3 dimensional of the antenna with gold cladding

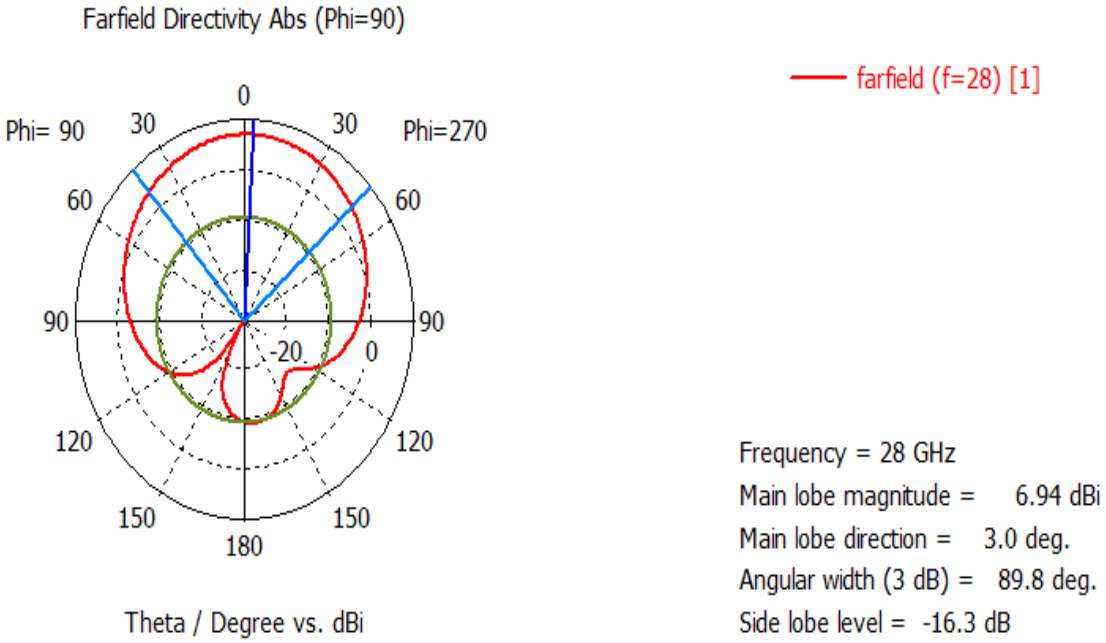

Figure 14-b

The far-field pattern in 2 dimensional (phi=90°) of the antenna with gold cladding

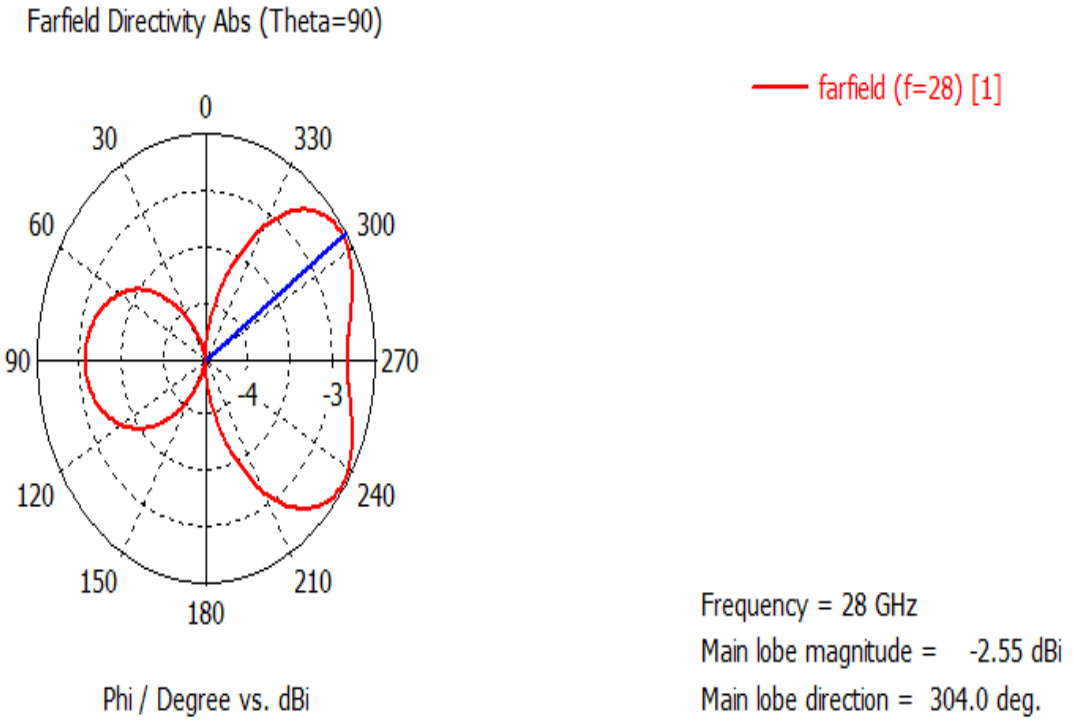

Figure 14-c

The far-field pattern in 2 dimensional (theta=90°) of the antenna with gold cladding

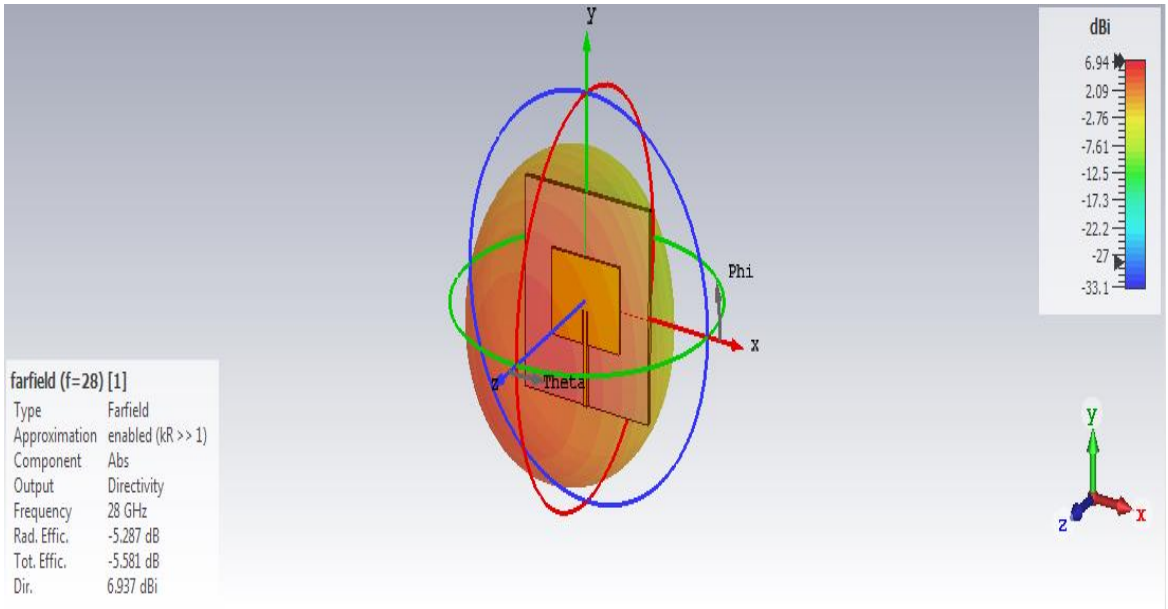

Figure 15-a
The far-field pattern in 3 dimensional of the antenna with silver cladding

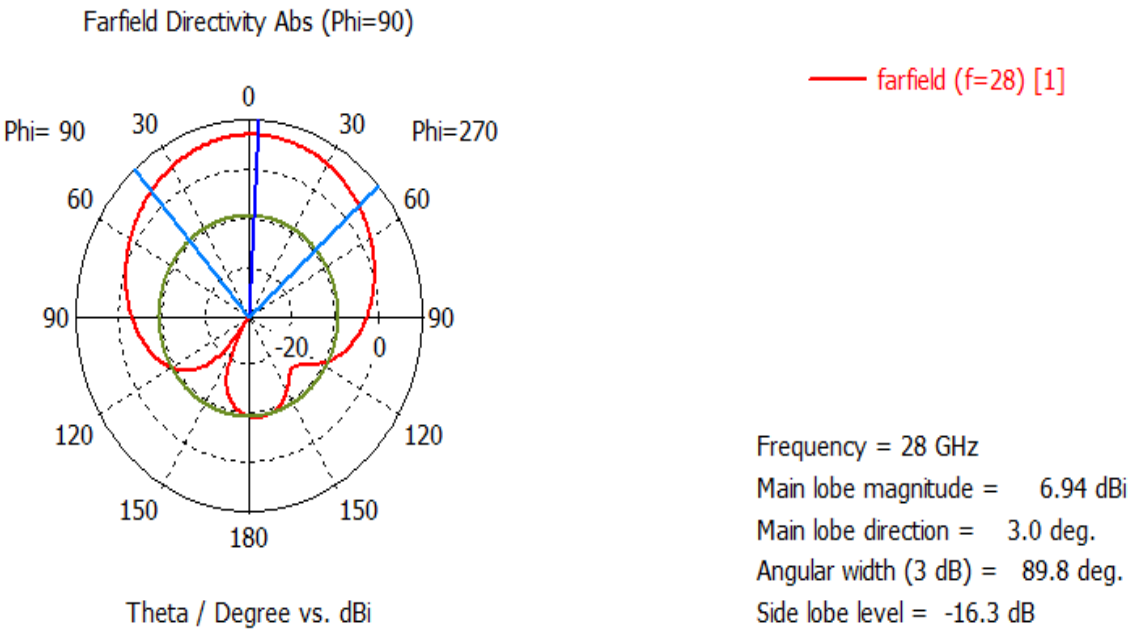

Figure 15-b
The far-field pattern in 2 dimensional (phi=90°) of the antenna with silver cladding

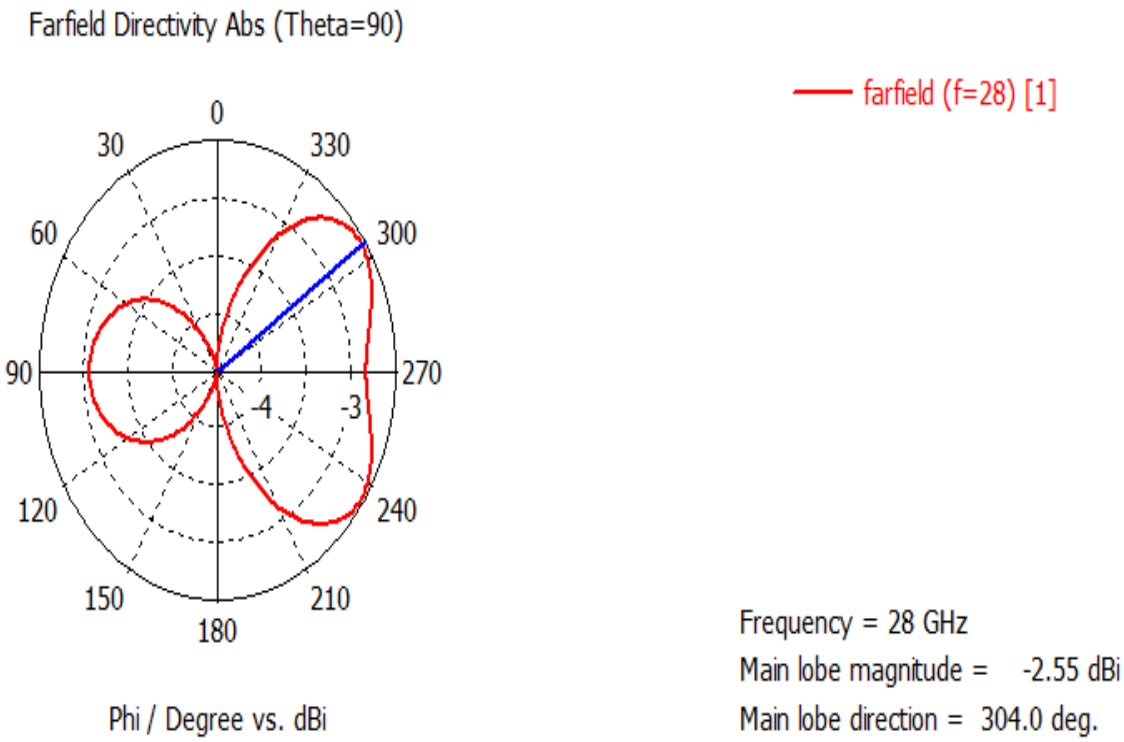

Figure 15-c
The far-field pattern in 2 dimensional (theta=90°) of the antenna with silver cladding

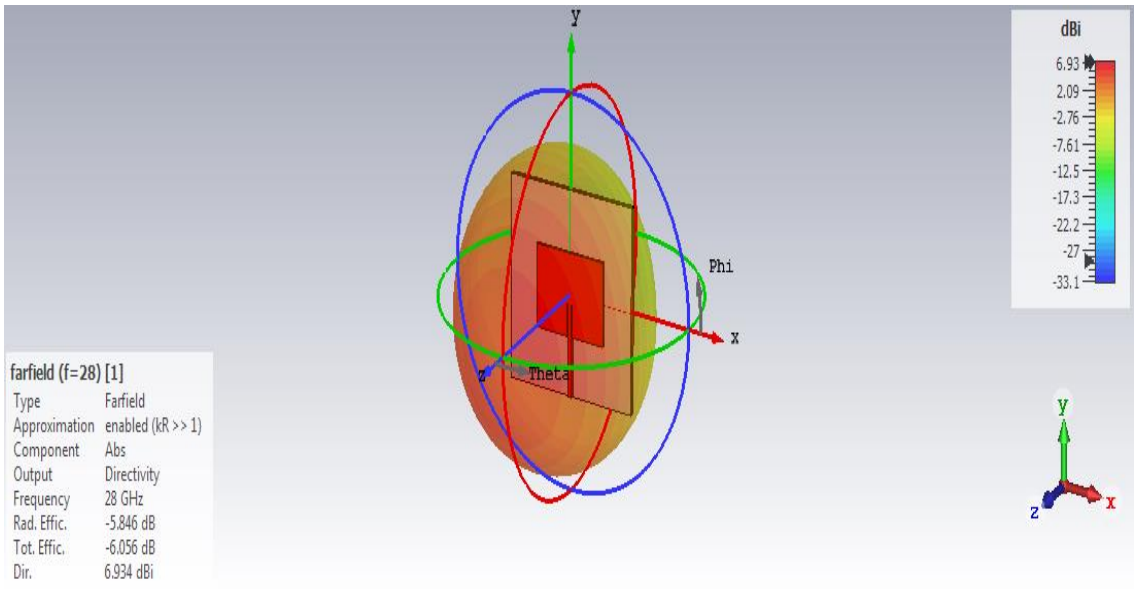

Figure 16-a
The far-field pattern in 3 dimensional of the antenna with iron cladding

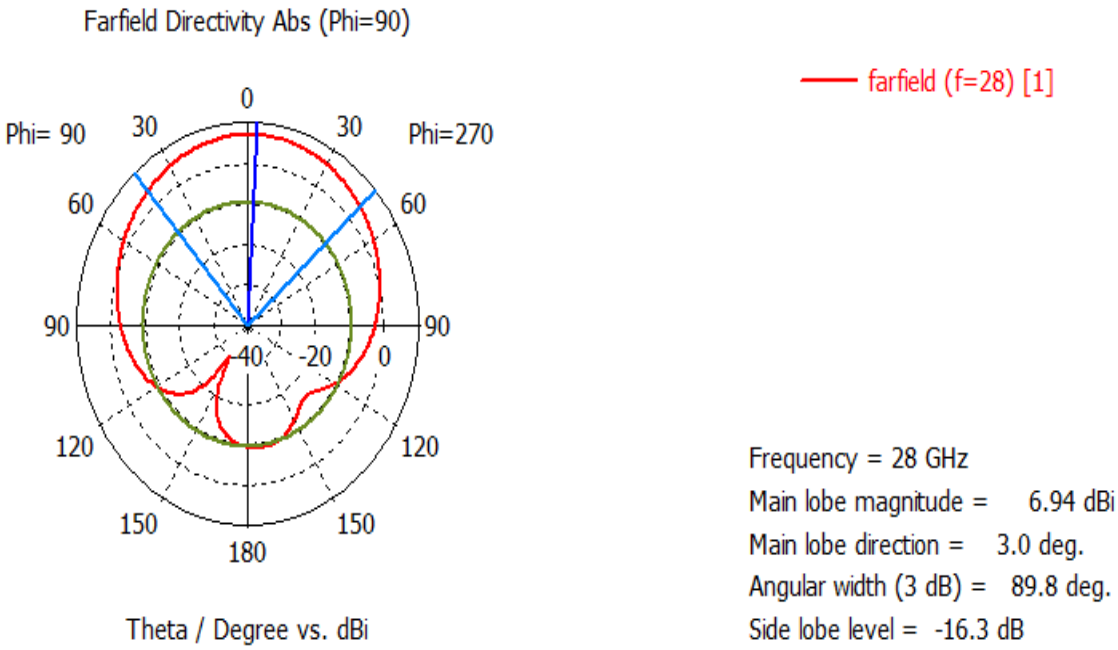

Figure 16-b

The far-field pattern in 2 dimensional (phi=90°) of the antenna with iron cladding

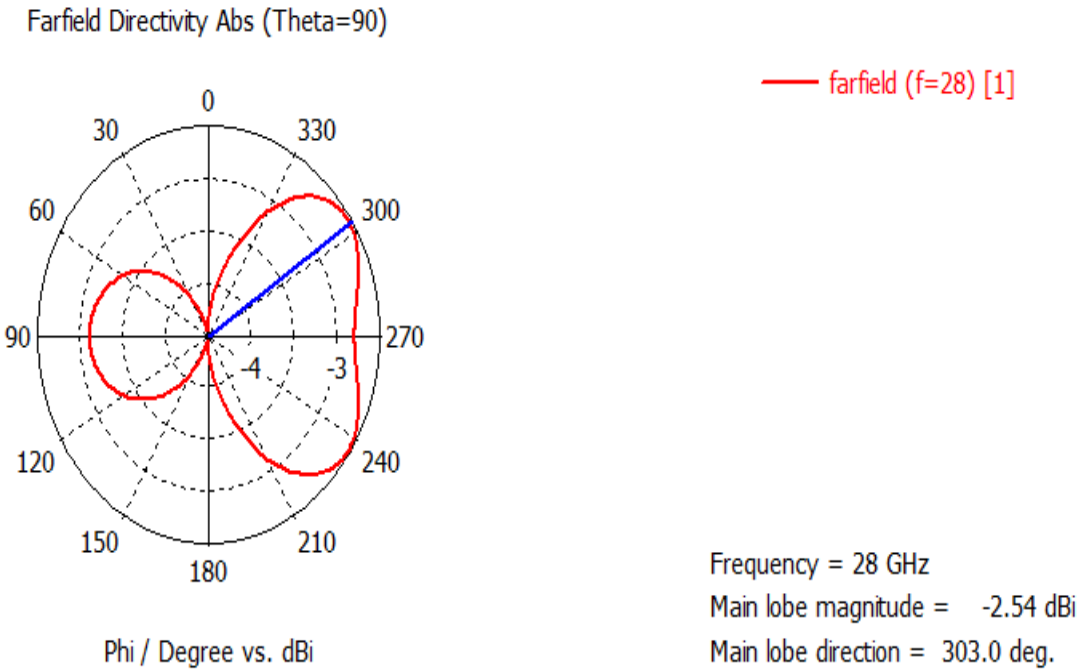

Figure 16-c

The far-field pattern in 2 dimensional (theta=90°) of the antenna with iron cladding

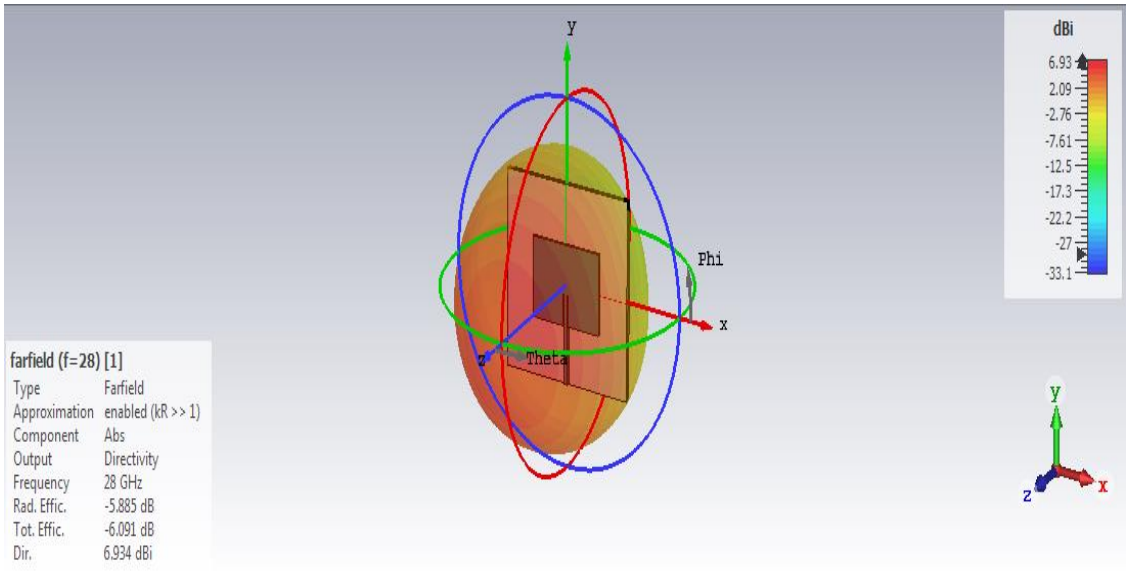

Figure 17-a

The far-field pattern in 3 dimensional of the antenna with platinum cladding

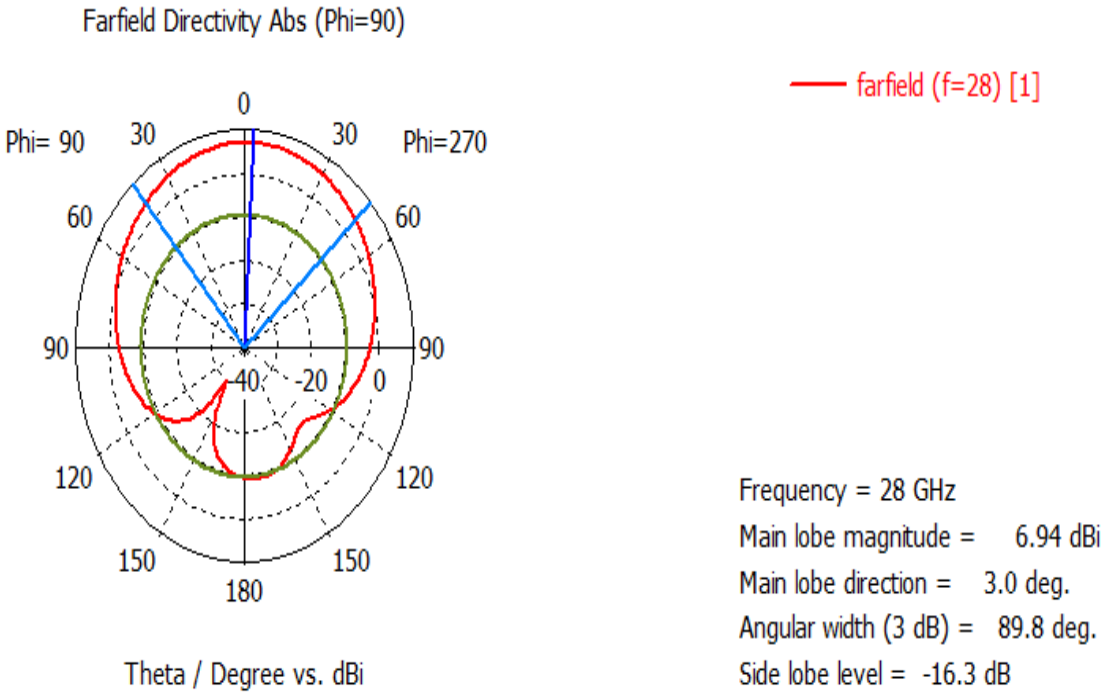

Figure 17-b

The far-field pattern in 2 dimensional (phi=90°) of the antenna with platinum cladding

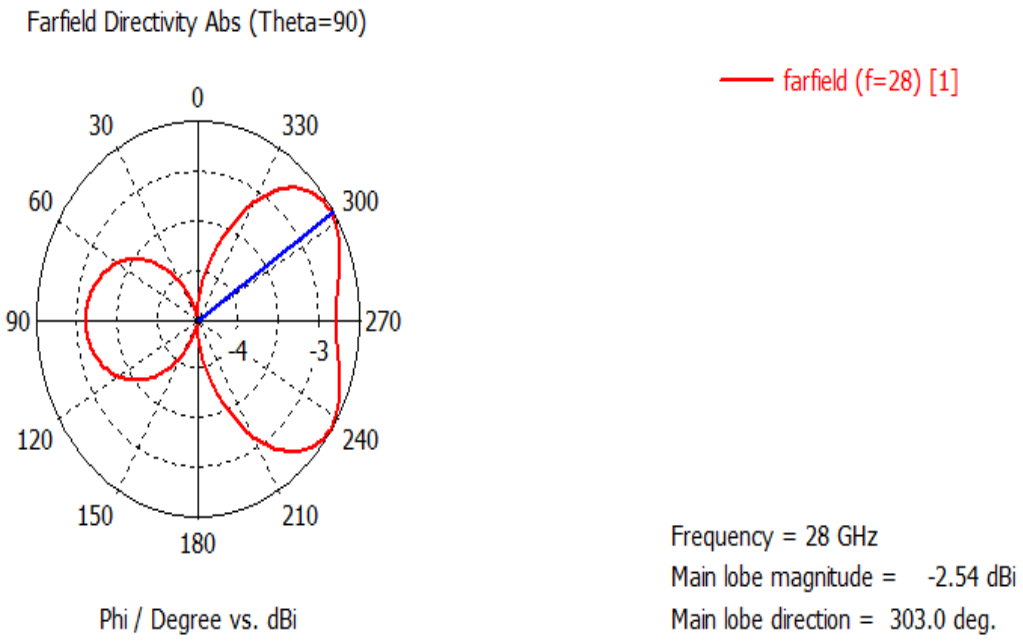

Figure 17-c

The far-field pattern in 2 dimensional (theta=90°) of the antenna with platinum cladding

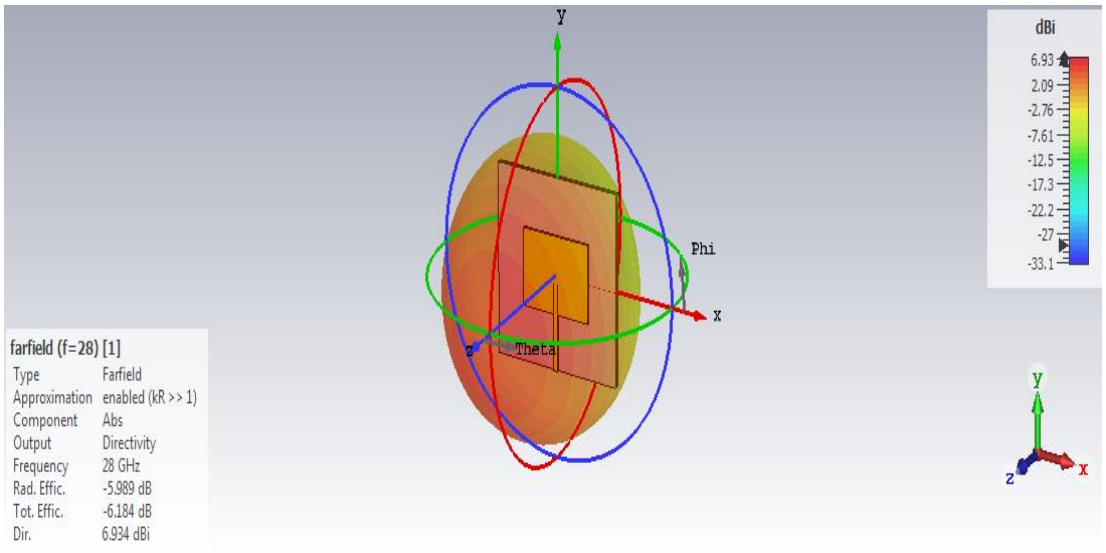

Figure 18-a

The far-field pattern in 3 dimensional of the antenna with tantalum cladding

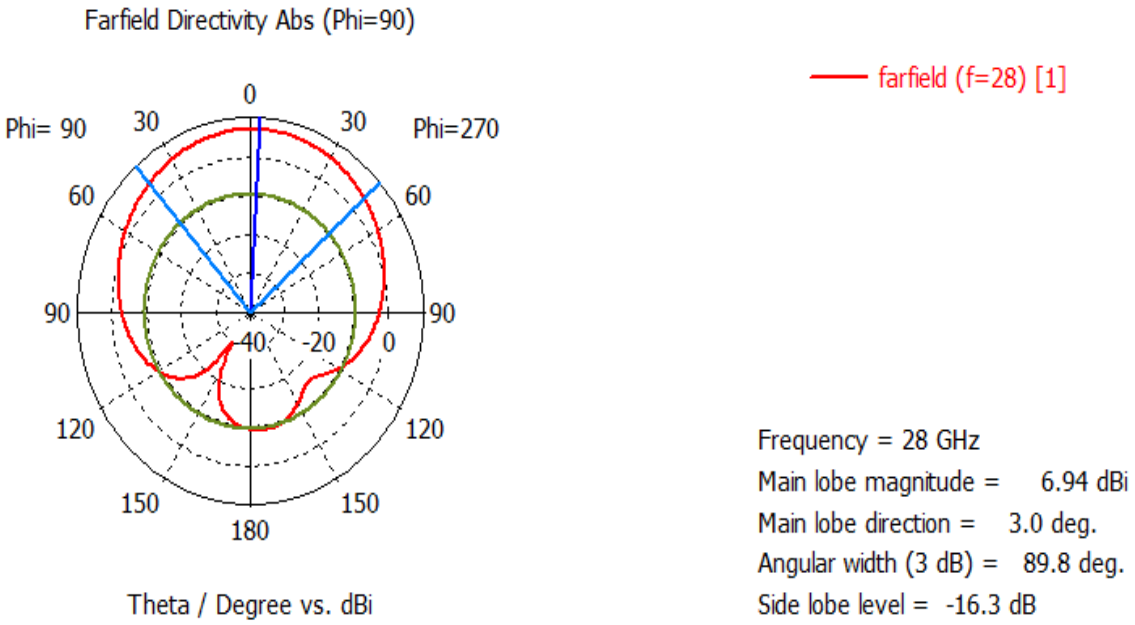

Figure 18-b

The far-field pattern in 2 dimensional (phi=90°) of the antenna with tantalum cladding

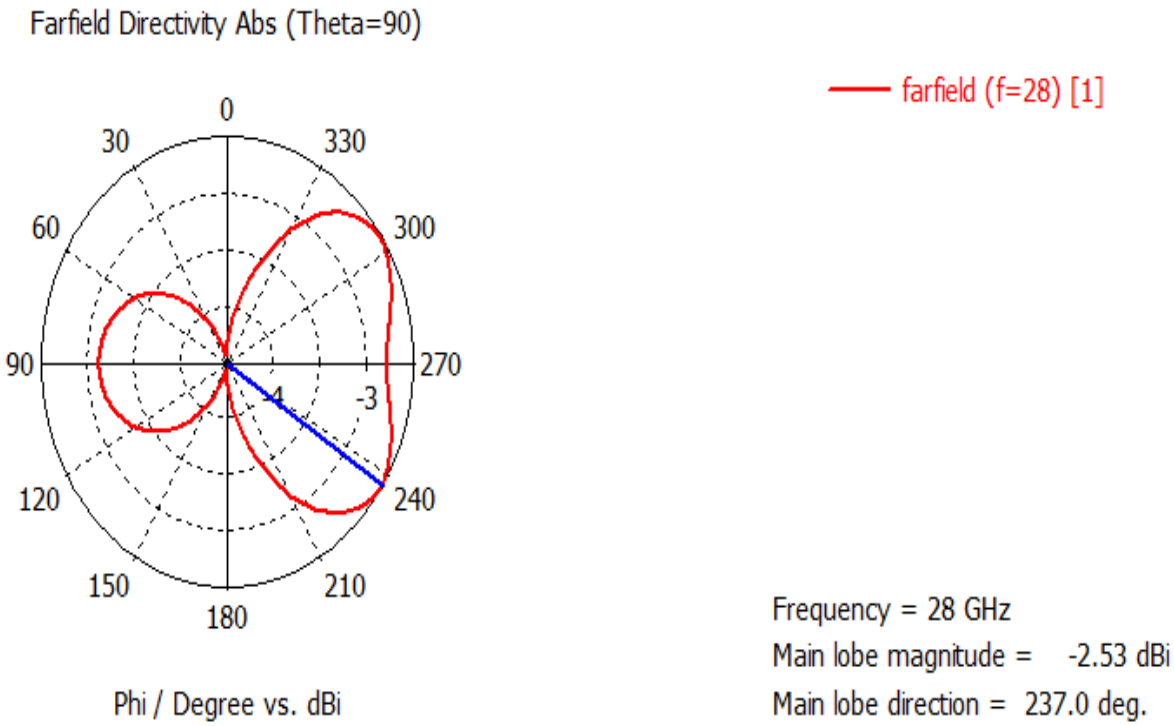

Figure 18-c

The far-field pattern in 2 dimensional (theta=90°) of the antenna with tantalum cladding

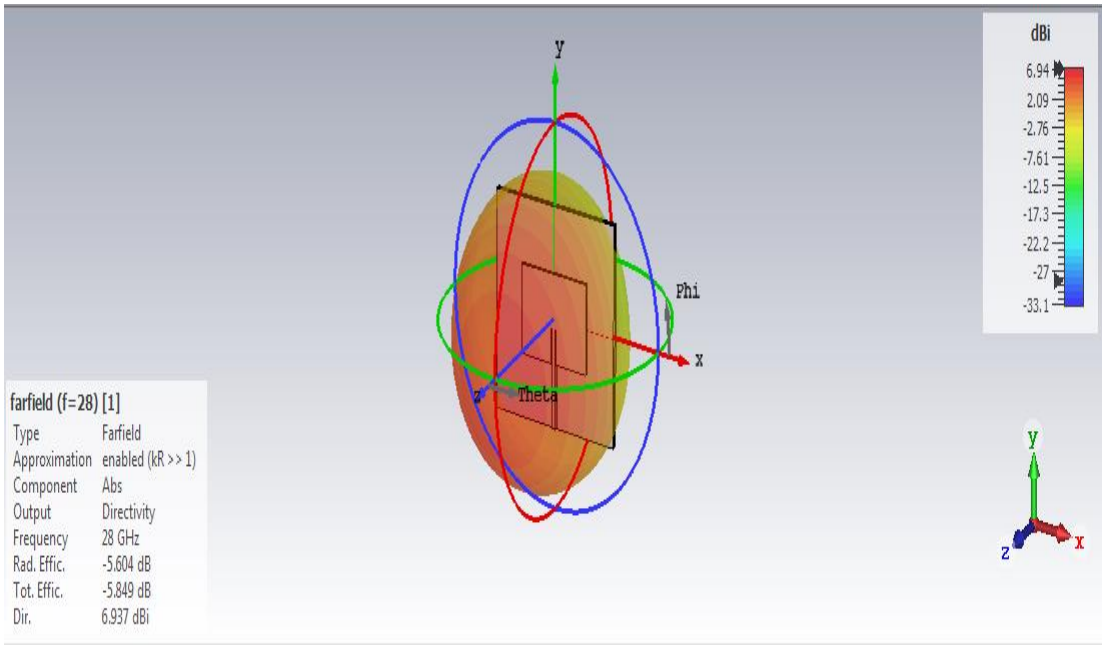

Figure 19-a

The far-field pattern in 3 dimensional of the antenna with molybdenum cladding

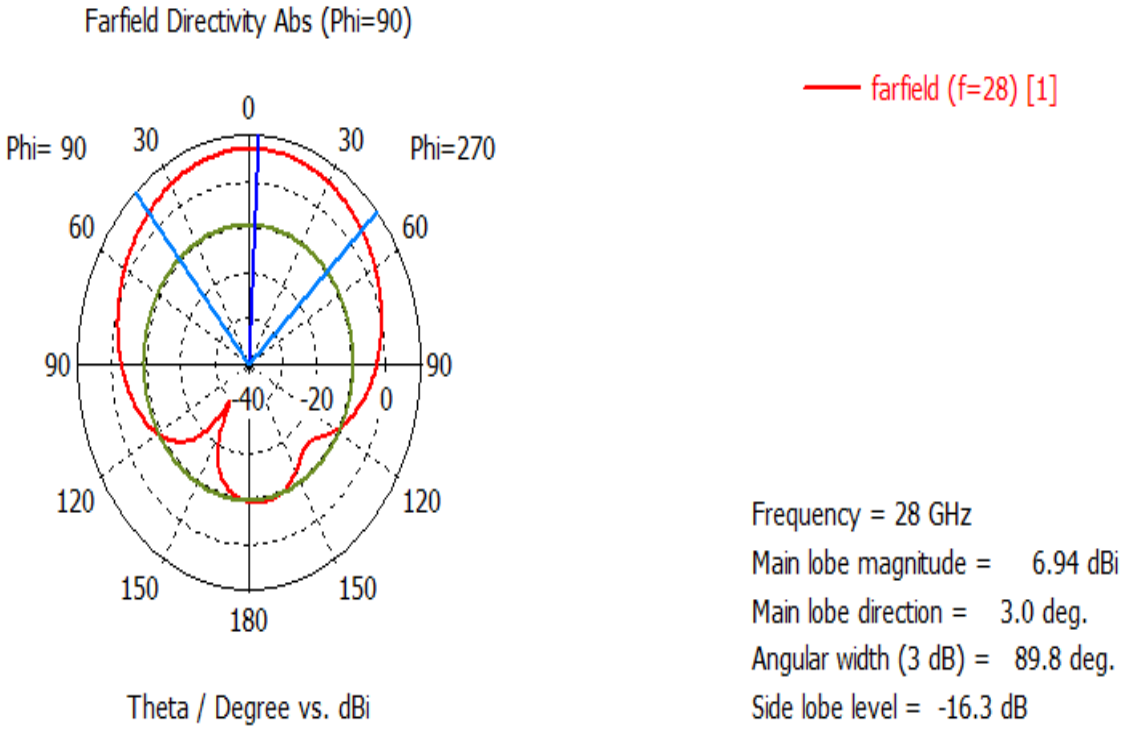

Figure 19-b

The far-field pattern in 2 dimensional (phi=90°) of the antenna with molybdenum cladding

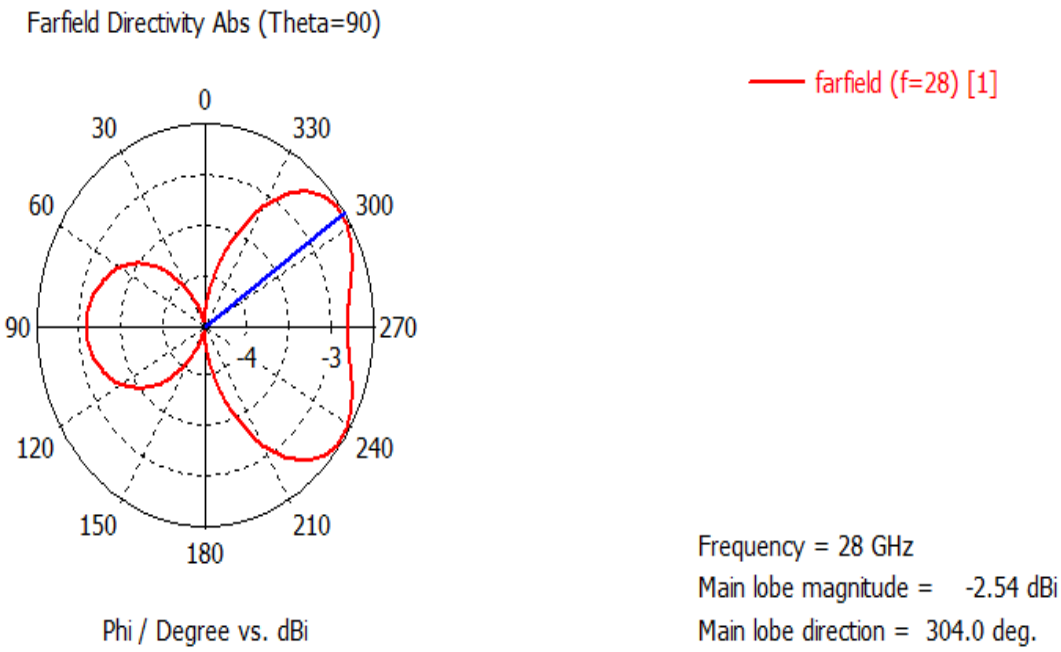

Figure 19-c

The far-field pattern in 2 dimensional (theta=90°) of the antenna with molybdenum cladding

The results are listed in Table 2 for evaluation.

Table 2. Comparison of antennas with different patch and ground conductors for antenna performance parameters

	Copper	Aluminum	Gold	Silver	Iron	Platinum	Tantalum	Molybdenum
Directivity (dBi)	6.937	6.937	6.937	6.937	6.934	6.934	6.934	6.937
Radiation Efficiency(dB)	-5.303	-5.415	-5.355	***-5.287***	-5.846	-5.885	-5.989	-5.604
Total Efficiency(dB)	-5.594	-5.687	-5.637	***-5.581***	-6.056	-6.091	-6.184	-5.849
Elevation Main-lobe Magnitude(dBi)	6.94	6.94	6.94	6.94	6.94	6.94	6.94	6.94
Elevation Main-lobe Direction(deg.)	3	3	3	3	3	3	3	3
3dB Elevation Angular Width(deg.)	89.8	89.8	89.8	89.8	89.8	89.8	89.8	89.8
Elevation Side-lobe Level (dB)	-16.3	-16.3	-16.3	-16.3	-16.3	-16.3	-16.3	-16.3
Azimuth Main-lobe Magnitude(dBi)	-2.55	-2.55	-2.55	-2.55	-2.54	-2.54	-2.53	-2.54
Azimuth Main-lobe Direction(deg.)	304	304	304	304	303	303	237	304

The results showed that the silver cladding had the best radiation and total efficiency at 28 GHz while the other performance parameters are about the same for all conductors used.

4. CONCLUSION

In this work, the rectangular patch microstrip antennas operating at 28 GHz frequency were designed for different patch conductors with the same dimensions. According to the design results, it has been seen that each of the patch conductors utilized has the potential to work in accordance with the desired operating frequency. The best performance due to the return loss criterion was tantalum conductor and the worst performance was obtained with a silver conductor. On the other hand, antenna efficiency performance was vice versa, that is, tantalum conductive was the worst while the silver conductor was the best. It is concluded that the loss of the silver-cladding antenna is less than the loss of the other cladding antennas used. This study is important in terms of predicting the effect of different patch claddings used in microstrip antennas on performance.

REFERENCES

1. Aguni, L., Chabaa, S., Ibnyaich, S. and Zeroual, A. (2019). Design of a Microstrip Patch Antenna for ISM band using Artificial Neural Networks, *Journal of Engineering Technology*, Vol 8, No 1, 97-113.

2. Ahmed, Z., Yang, K., McEvoy, P. and Ammann, M.J., (2017). Study of mm-Wave Microstrip Patch Array on Curved Substrate. *Loughborough Antennas & Propagation Conference (LAPC), Loughborough, UK*, 1-4.

3. Balanis, C.A. (2016). *Antenna Theory: Analysis and Design*, John Wiley&Sons Ltd.

4. Bhanumathi, V. and Swathi, S. (2019). Bandwidth Enhanced Microstrip Patch Antenna for UWB Applications, *ICTACT Journal on Microelectronics*, Vol 4, No 4, 669-675. DOI: 10.21917/ijme.2019.01116.

5. Garg, R., Bhartia, P., Bahl, I. and Ittipiboon, A. (2001). *Microstrip Design Antenna* Handbook, Artech House, Inc.

6. Islam, Md.M., Hasan, R.R., Rahman, Md. M., Islam, K.S. and Al-Amin, S.M. (2016), Design & Analysis of Microstrip Patch Antenna Using Different Dielectric Materials for WiMAX Communication System. *The International Journal of Engineering & Science*, 4, 20-21. DOI:10.3991/ijes.v4i1.5569.

7. Khalily, M., Rahman, T.A. and Kamarudin, M.R. (2016). Design of Phased Arrays of Series-Fed Patch Antennas with Reduced Number of the Controllers for 28 GHz mm-Wave Applications, *IEEE Antennas and Wireless Propagation Letters*, Vol 15, 1305-1308. DOI:10.1109/LAWP.2015.2505781.

8. Kiran, T., Mounisha, N., Ch.Mythily, Akhil, D. and Kumar, T.V.B.P. (2018). Design of Microstrip Patch Antenna for 5g Applications, *IOSR Journal of Electronics and Communication Engineering (IOSR-JECE)*, Vol 13, No 1, 14-17. DOI: 10.9790/2834-1301011417.

9. Mahabub, A., Rahman, M.M., Al-Amin, M., Rahman, M.S. and Rana, M.M. (2018). Design of a Multiband Patch Antenna for 5G Communication Systems, *Open Journal of Antennas and Propagation*, 1-14. DOI: 10.4236/ojapr.2018.61001.

10. Matin, M. A. and Sayeed, A. I. (2010). A design rule for inset-fed rectangular microstrip patch antenna, *Wseas Transactions on Communications*, 1(9), 63-72.

11. Mondal, K. and Sarkar, P. P. (2019). Gain and Bandwidth Enhancement of Microstrip Patch Antenna for WiMAX and WLAN Applications, *IETE Journal of Research*, 1-9. DOI: 10.1080/03772063.2019.1565958.

12. Nakar, P. S., (2004). *Design of a Compact Microstrip Patch Antenna for Use in Wireless/Cellular Devices.* The Florida State University College of Engineering Master of Thesis, Retrieved from http://purl.flvc.org/fsu/fd/FSU_migr_etd-2790.

13. Parchin, N.O., Shen, M. and Pedersen,G.F., (2016). End-Fire Phased Array 5G Antenna Design Using Leaf-Shaped Bow-Tie Elements for 28/38 GHz MIMO Applications, *2016 IEEE International Conference Ubiquitous Wireless Broadband (ICUWB)*, 1-4. DOI: 10.1109/ICUWB.2016.7790538.

14. Pozar, D.M. (2012). *Microwave Engineering*, John Wiley & Sons, Inc.

15. Rodriguez, J. (2015). *Fundamentals of 5G Mobile Networks*, John Wiley&Sons Ltd. DOI:10.1002/9781118867464.

16. Sethi, W.T., Ashraf, M.A., Ragheb, A., Alasaad, A. and Alshebeili, S.A. (2018). Demonstration of Millimeter Wave 5G Setup Employing High-Gain Vivaldi Array, *Hindawi International Journal of Antennas and Propagation*. Vol. 2018, 12 pages. DOI: 10.1155/2018/3927153.

17. Verma, S., Mahajan, L., Kumar, R., Saini, H.S. and Kumar, N. (2016). A Small Microstrip Patch Antenna for Future 5G Applications. *5th International Conference on Reliability, Infocom Technologies and Optimization (ICRITO) (Trends and Future Directions)*, Sep. 7-9, AIIT, Amity University Uttar Pradesh, Noida, India. DOI: 10.1109/ICRITO.2016.7784999.

18. Yoon, N. and Seo, C. (2017). A 28 GHz Wideband 2x2 U-Slot Patch Array Antenna, *Journal of Electromagnetic Engineering and Science*, 17, 133-137. DOI: 10.5515/JKIEES.2017.17.3.133.